P_s = average prestress pressure on prestressing plate;
Q = pull out force;
Q_f = ultimate pull out force;
q_i = individual anchor load;
S = anchor spacing in widths or diameters;
V = volume of annulus;
γ = sand density;
Δ = uplift displacement;
Δ_s = settlement of surface prestressing plate; and
Φ = angle of internal friction.

JOURNAL OF THE SOIL MECHANICS AND FOUNDATIONS DIVISION

Influence of Progressive Failure on Slope Stability

By Fredy Romani,[1] A. M. ASCE, C. William Lovell, Jr.,[2] M. ASCE, and Milton E. Harr,[3] F. ASCE

INTRODUCTION

Most types of slope failure demonstrate a distinctly progressive character (6). According to Bjerrum (4), progressive failure will be obtained in a slope (of overconsolidated clay) if successively, at points along a potential failure surface, the simultaneous satisfaction of three criteria is obtained: (1) There must be large internal stresses in the clay mass; (2) the material must have a stress-strain curve exhibiting a substantial peak, i.e., become strain softening; and (3) there must be enough energy to strain the material beyond this peak.

There is a considerable interest within solid mechanics in the propagation of cracks and their consequent effects. Analysis for stresses and strains in cracked bodies is reduced in complexity if the shape and position of the crack are assumed, as is usual in the search for a critical sliding surface in assessing the stability of slopes. In such cases, stability is progressively decreased as zones of critical stress level develop. Observations in the field (6) indicate preferred points of crack initiation and directions of propagation. Current slope stability procedures vary, but basically they ignore the effects of cracking prior to total failure of the soil mass, or treat them in an empirical manner (7).

The purpose herein is to present a method for evaluating the effects of

Note.—Discussion open until April 1, 1973. To extend the closing date one month, a written request must be filed with the Editor of Technical Publications, ASCE. This paper is part of the copyrighted Journal of the Soil Mechanics and Foundations Division, Proceedings of the American Society of Civil Engineers, Vol. 98, No. SM11, November, 1972. Manuscript was submitted for review for possible publication on September 28, 1971.

[1]Sr. Engr., National Soil Services, Inc., Houston, Tex.
[2]Prof. of Civ. Engrg., Purdue University, Lafayette, Ind.
[3]Prof. of Soil Mechanics, Purdue University, Lafayette, Ind.

crack propagation in soil bodies with sloping boundaries. The following first assumptions are applied: the body is a linear elastic material, the problem is two-dimensional, and the most critical sliding surface within the body progresses along a circular path which passes through the toe of the slope.

THEORETICAL CONSIDERATIONS

Of the methods available for the analysis of the stability of slopes, the most significant for practical applications are those based on the assumption of a surface of rupture separating two essentially rigid bodies (12). The shape of the surface of rupture is chosen somewhat arbitrarily, and the most critical position of it is determined by a procedure of trial and error.

The methods of slices (2) belong in the preceding category and enjoy wide acceptance in current practice. They exist in several versions, depending on the assumption made with respect to the distribution of forces within the

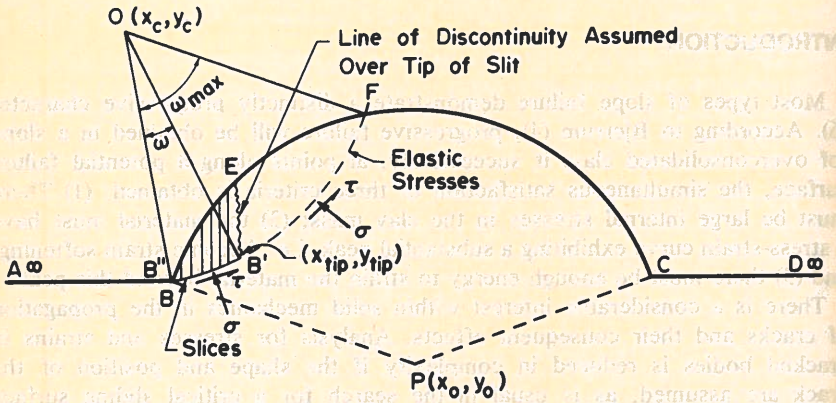

Fig. 1.—Slope Stability Analysis for Elastic Circular Embankment with Circular Slit

soil mass. The rupture is assumed to occur simultaneously along a most critical surface in the material of reduced strength, i.e., the factor of safety at each point along a given surface at a given time is constant. The effects of progressive cracking and an average factor of safety which varies with time are not well understood.

The approach used in this study of progressive failure is shown in Fig. 1. The body to be analyzed for stress and slope stability has a cylindrical upper boundary, and may contain a cylindrical slit or discontinuity. By appropriate selection of $P(x_o, y_o)$, embankment dimensions may be suitably approximated; the circular cross section is chosen only for mathematical convenience. With the application of a simplified method of slices, the factor of safety may be determined for any desired degree of development of the circular discontinuity.

The method for determining elastic stresses and strains in such bodies has been explained in detail elsewhere (9,10,11). Briefly stated, the method

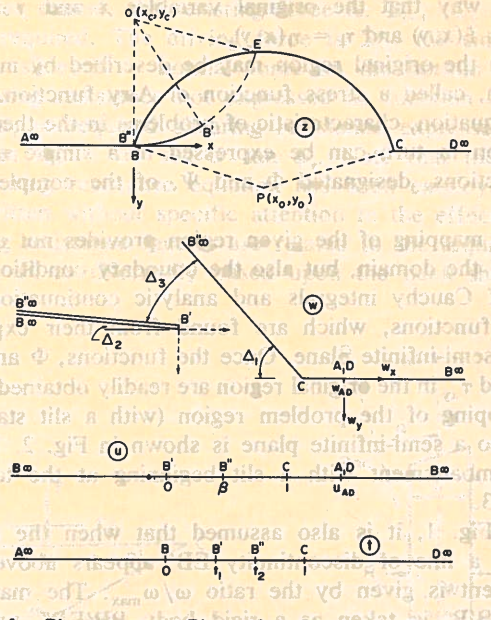

Fig. 2.—Mapping of *z*-Plane onto *t*-Plane for Case of Slit Originating at Toe of Slope

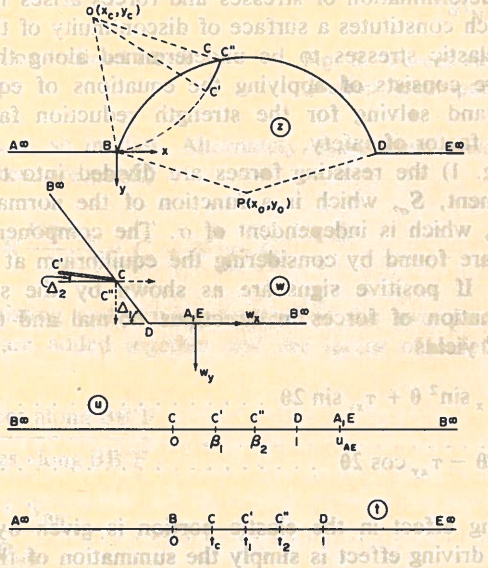

Fig. 3.—Mapping of *z*-Plane onto *t*-Plane for the Case of Slit Originating at Top of Slope

obtains the conformal transformation of the original region onto a semi-infinite plane in such a way that the original variables x and y are replaced by ξ and η, with $\xi = \xi(x, y)$ and $\eta = \eta(x, y)$.

The stresses in the original region may be described by means of a single auxiliary function, called a stress function or Airy function, which satisfies the biharmonic equation, characteristic of problems in the theory of elasticity. The Airy function in turn can be expressed in a simple manner with the help of two functions, designated Φ and Ψ, of the complex variable, $z = x + iy$.

The conformal mapping of the given region provides not only a geometric transformation of the domain, but also the boundary conditions. Use is made of the theory of Cauchy integrals and analytic continuation to obtain the unknown stress functions, which are found from their expressions at the boundary of the semi-infinite plane. Once the functions, Φ and Ψ, are found, stresses σ_y, σ_x and τ_{xy} in the original region are readily obtained. The successive steps in the mapping of the problem region (with a slit starting at the toe of the slope) onto a semi-infinite plane is shown in Fig. 2. The similar case for a circular embankment with a slit beginning at the top of the slope is shown in Fig. 3.

As shown in Fig. 1, it is also assumed that when the slit advances to a givenpoint B′, a line of discontinuity EB′ appears above it. The extent of slit development is given by the ratio ω/ω_{max}. The material above the circular crack BB′B″ is taken as a rigid body BB′EB″, whose stability is analyzed by a simple method of slices. The region to the right (B′FE) is assumed to be in a condition of elastic stress. The need for this mixed approach to the determination of stresses and forces arises from the circular crack BB′B″, which constitutes a surface of discontinuity of the stress vector, and causes the elastic stresses to be undetermined along that surface. The solution procedure consists of applying the equations of equilibrium to the body BB′FEB″, and solving for the strength reduction factor, commonly interpreted as the factor of safety.

Along B′F (Fig. 1) the resisting forces are divided into two components, namely a component, S_σ, which is a function of the normal stress, σ, and a component, S_c, which is independent of σ. The components of the stress vectors σ and τ are found by considering the equilibrium at any point along the surface B′F. If positive signs are as shown by the stress vectors in Fig. 4, the summation of forces in directions normal and tangential to the inclined plane BC yields

$$\sigma = \sigma_y \cos^2\theta + \sigma_x \sin^2\theta + \tau_{xy} \sin 2\theta \quad \ldots\ldots (1)$$

$$\tau = \frac{\sigma_y - \sigma_x}{2} \sin 2\theta - \tau_{xy} \cos 2\theta \quad \ldots\ldots (2)$$

Thus, the resisting effect in the elastic portion is given by $\tan\phi_a \int_{B'}^{F} \sigma\, ds + c_a \int_{B'}^{F} ds$. The driving effect is simply the summation of the driving forces $\int_{B'}^{F} \tau\, ds$ along the path B′F.

The remaining part of the analysis is accomplished by a method of slices, with the Bishop simplification as shown in Fig. 5, i.e., R_R and R_L are horizontal.

Taking the sums for all n slices, and recognizing that the forces on the sides of the slices cancel, the resisting force is: $\Sigma_{i=1}^{n} (C_r + N \tan\phi_r)$, in which r means required. The driving force is: $\Sigma_{i=1}^{n} (W \sin\alpha)$ in which W = weight of the slice; N = normal force on the bottom of the slice; C_r = required shearing resistance not expressed as function of N; $C_r = c_r b \sec\alpha$; $N \tan\phi_r$ = required shearing resistance expressed as a function of N; and $N \tan\phi_r = \sigma b \sec\alpha \tan\phi_r$. Note that the Mohr-Coulomb form of the shearing resistance equation has been employed, and that the equations are written without specific attention to the effects of water. The available shearing resistance factors are related to the required ones by the factor of safety, F, as (Normally based upon the peak shearing resistance

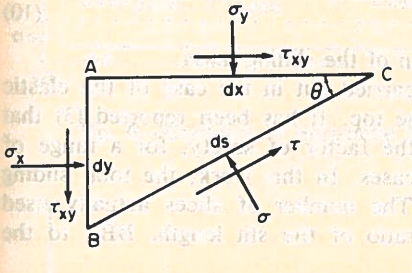

Fig. 4.—Stresses on Inclined Plane

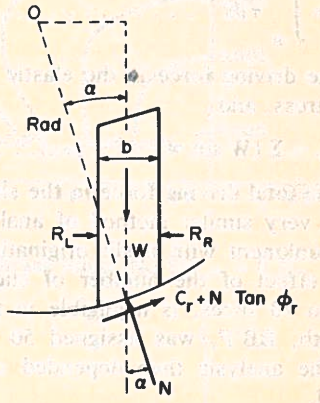

Fig. 5.—Forces Acting on Slice (Bishop Assumption)

and the subscript, a, so implies. Alternately, parameters based upon residual values, subscript res, are used.)

$$S_r = \frac{S_a}{F} = \frac{C_a}{F} + N\frac{\tan\phi_a}{F} = C_r + N\tan\phi_r \quad \ldots\ldots (3)$$

Finally, the resisting and driving forces for the two parts considered in the sliding mass are added together and the factor of safety is determined by

$$F = \frac{\text{Resisting forces along BB′F}}{\text{Driving forces along BB′F}} \quad \ldots\ldots (4)$$

or $$F = \frac{S_\sigma + S_c + S_{BB'}}{D_\tau + D_{BB'}} \quad \ldots\ldots (5)$$

in which $$S_\sigma = \tan\phi_a \int_{B'}^{F} \sigma\, ds \quad \ldots\ldots (6)$$

which equals available shearing resistance force in the elastic part dependent upon the normal component of stress; and

$$S_c = c_a \int_{B'}^{F} ds \quad \ldots\ldots (7)$$

which is available shearing resistance force in the elastic part independent of the normal component of stress, and

$$S_{BB'} = \sum [C_a + N \tan \phi_a] \quad \ldots\ldots (8)$$

which equals available shearing resistance force in the slit portion of the mass; and

$$D_\tau = \int_{B'}^{F} \tau\, ds \quad \ldots\ldots (9)$$

is the driving force in the elastic part which induces the shearing components of stress; and

$$D_{BB'} = \Sigma\,(W \sin \alpha) \quad \ldots\ldots (10)$$

is the total driving force in the slit portion of the sliding mass.

A very similar method of analysis is carried out in the case of the elastic embankment with a slit originating at the top. It has been reported (3) that the effect of the number of slices on the factor of safety, for a range of 15 to 70 slices, is negligible in typical cases. In this work, the total sliding length, BB′F, was assigned 50 slices. The number of slices actually used in the analysis then depended on the ratio of the slit length, BB′, to the total.

RESULTS

Stress Distribution.—The stress distribution within and under long, linear elastic, isotropic, homogeneous, and circular embankments continuous with the underlying material and containing a crack of circular shape was investigated. Only body forces due to gravity were considered, including those below the base of the embankment. In similar investigations (1,10), the material below the base of the embankment was assumed to be weightless. Embankment proportions, viz, width-height ratios were taken at practical levels. The calculated stress distributions were tested at random by checking equilibrium of partial areas of the embankment.

No Slit.—Figs. 6 through 9 show typical distributions of stress for an embankment of given geometry and physical parameters. The contours represent stresses in a dimensionless form, viz., stress/γH, in which γ = unit weight and H is the maximum (center) height of the embankment. In Figs. 6 and 8 the value of Poisson's ratio μ is 0.3, while in Figs. 7 and 9, μ = 0.475. Prior reported studies suggest that μ = 0.3 is a reasonable value for unsaturated soils, while μ = 0.475 is a value appropriate to a saturated clay (5).

The values of vertical normal stress are rather insensitive to changes in Poisson's ratio. A change in the value of μ from 0.3 to 0.475 causes a variation in the values of the vertical normal stresses of less than 5 %; this conclusion was also reported by Perloff, et al. (10).

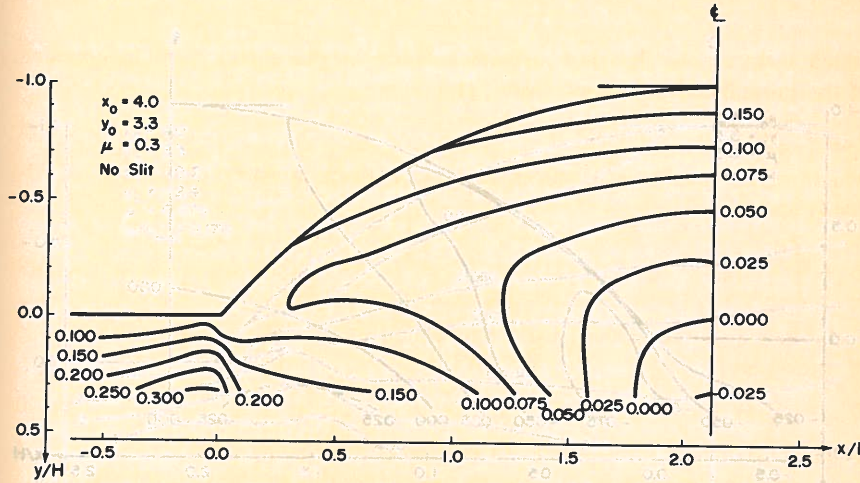

Fig. 6.—Contours of Horizontal Normal Stress Ratio (No Slit μ = 0.3)

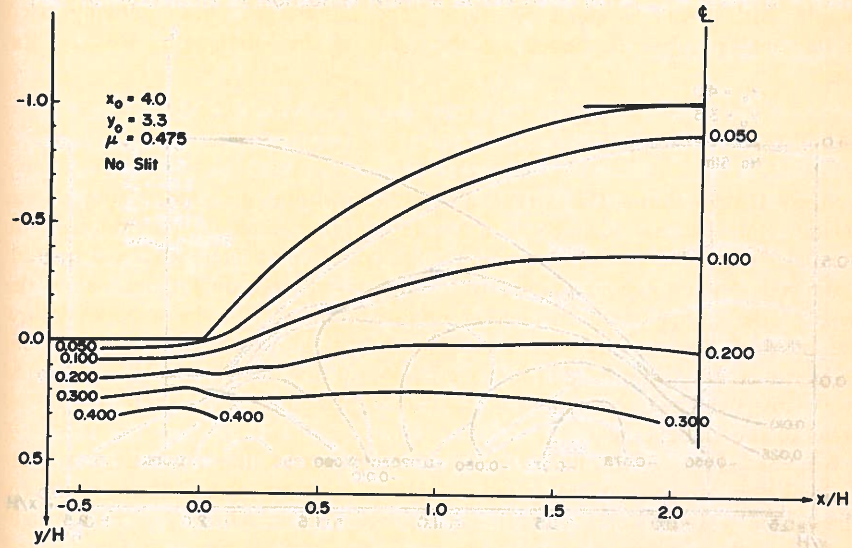

Fig. 7.—Contours of Horizontal Normal Stress Ratio (No Slit; μ = 0.475)

Contours of horizontal normal stress ratio $\sigma_x/\gamma H$ are shown in Figs. 6 and 7. For these, and contrary to the case of vertical normal stresses, a change in the value of Poisson's ratio from 0.3 to 0.475 produces a very

different pattern of stresses, both in magnitude and distribution. When $\mu = 0.3$, the horizontal normal stresses tend to change more rapidly near the toe of the slope. Values of these stresses at the center line of the embankment

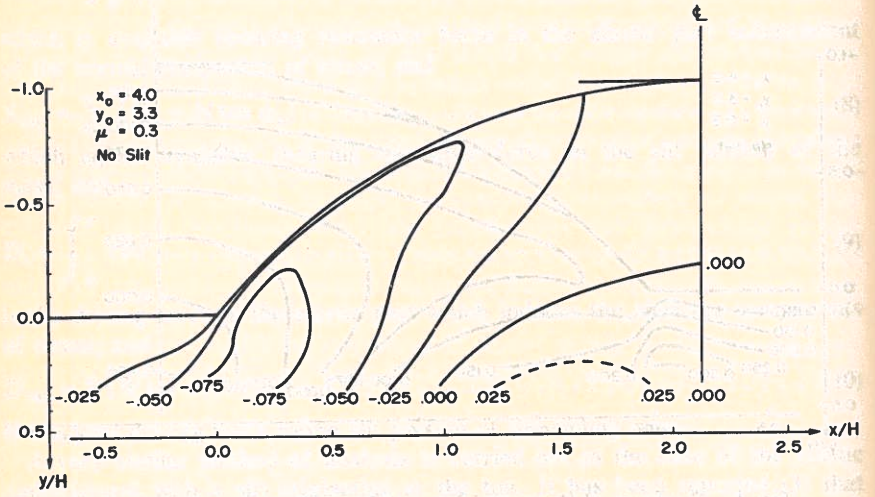

Fig. 8.—Contours of Shear Stress Ratio (No Slit; $\mu = 0.3$)

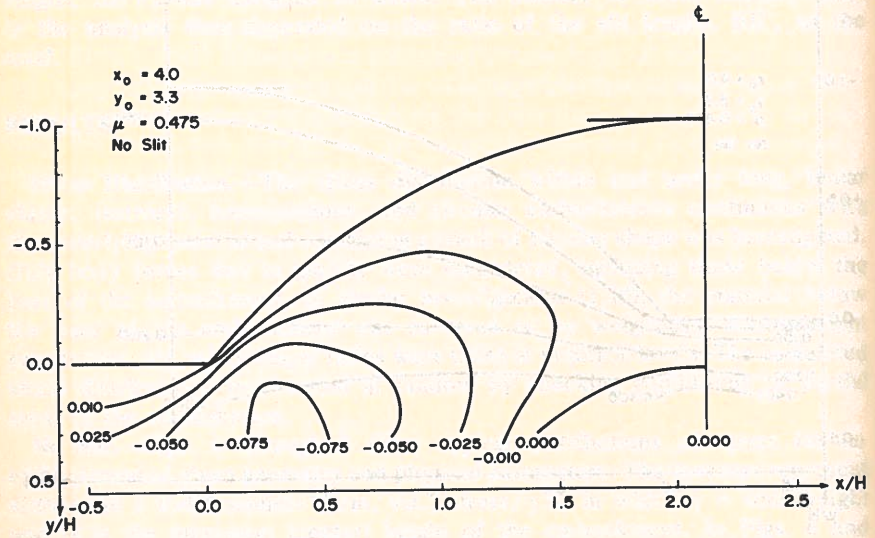

Fig. 9.—Contours of Shear Stress Ratio (No Slit; $\mu = 0.475$)

decrease in magnitude with depth for $\mu = 0.3$, but increase for $\mu = 0.475$. In the case of $\mu = 0.3$, a slight area of tension is seen to develop within the embankment. The area in which tension is in evidence was found to

increase in size within and under the embankment as the ratio (y_o/x_o) of the coordinates of the center of the circle defining the boundary of the embankment increases. A value of $y_o/x_o = 0.85$ seems to be critical, i.e.,

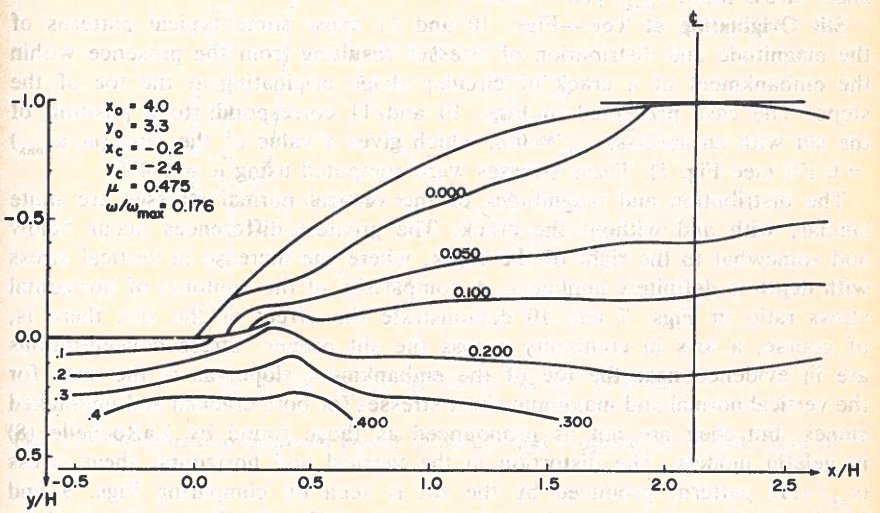

Fig. 10.—Contours of Horizontal Normal Stress Ratio ($\omega/\omega_{max} = 0.176$; $\mu = 0.475$)

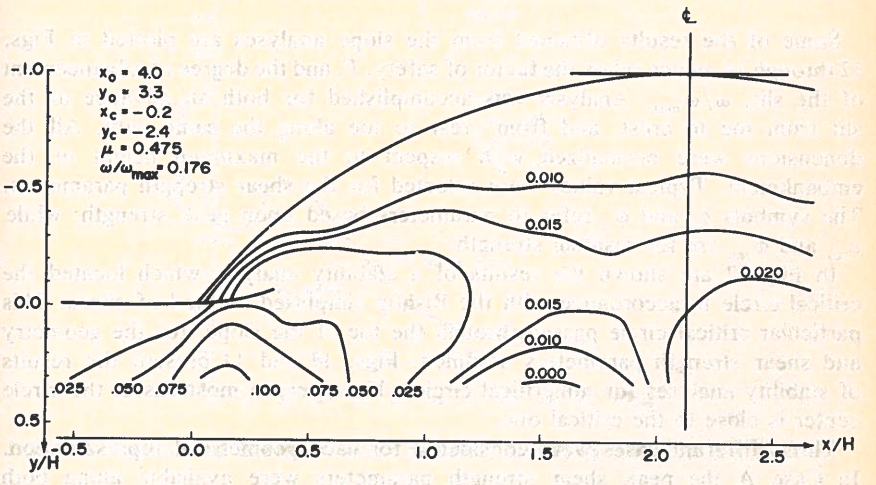

Fig. 11.—Contours of Shear Stress Ratio ($\omega/\omega_{max} = 0.176$; $\mu = 0.475$)

for values of $y_o/x_o > 0.85$, only compressive horizontal normal stresses are calculated within the embankment. When a value of $\mu = 0.475$ is used, the contours of $\sigma_x/\gamma H$ display a flatter orientation.

Figs. 8 and 9 show contours of shear stress ratio for $\mu = 0.3$ and $\mu = 0.475$. As for the horizontal normal stress, the pattern of stress distribution is changed by the value of μ, but to a lesser degree. However, this change in Poisson's ratio led to only a small change in the distribution of the maximum shear stress ratio, $\tau_{max}/\gamma H$.

Slit Originating at Toe.—Figs. 10 and 11 show some typical patterns of the magnitude and distribution of stresses resulting from the presence within the embankment of a crack of circular shape originating at the toe of the slope. The case presented in Figs. 10 and 11 corresponds to a position of the slit with an abscissa $x_{tip} = 0.6$, which gives a value of the ratio $(\omega/\omega_{max}) = 0.176$ (see Fig. 1). These stresses were computed using $\mu = 0.475$.

The distribution and magnitudes of the vertical normal stresses are quite similar, with and without the crack. The greatest differences occur below and somewhat to the right of the crack, where the increase in vertical stress with depth is definitely nonlinear. A comparison of the contours of horizontal stress ratio in Figs. 7 and 10 demonstrate the effect of the slit; there is, of course, a loss in continuity across the slit proper. Stress concentrations are in evidence near the toe of the embankment slope, as is the case for the vertical normal and maximum shear stresses for both cracked and uncracked slopes, but they are not as pronounced as those found by LaRochelle (8) in gelatin models. The distortion in the vertical and horizontal shear stress $(\tau_{xy}/\gamma H)$ pattern, produced by the slit is seen by comparing Figs. 9 and 11. Again, the contours are discontinuous across the slit. The maximum shear stress ratio $\tau_{max}/\gamma H$ is only locally modified by the presence of the slit.

STABILITY ANALYSIS

Some of the results obtained from the slope analyses are plotted in Figs. 12 through 14, which relate the factor of safety, F, and the degree of advancement of the slit, ω/ω_{max}. Analysis was accomplished for both an advance of the slit from toe to crest, and from crest to toe along the same path. All the dimensions were normalized with respect to the maximum height of the embankment. Typical values were selected for the shear strength parameters. The symbols c_a and ϕ_a refer to parameters based upon peak strength; while c_{res} and ϕ_{res} are for residual strength.

In Fig. 12 are shown the results of a stability analysis which located the critical circle in accordance with the Bishop simplified method of slices. This particular critical circle passed through the toe of the slope, for the geometry and shear strength parameters assumed. Figs. 13 and 14 present the results of stability analyses for noncritical circles. However, in most cases, the circle center is close to the critical one.

Three different cases were considered for each geometrical representation. In Case A the peak shear strength parameters were available along both the failed and nonfailed portions of the assumed critical surface (Fig. 12). In Case B peak values of shear strength parameters were available along the nonfailed portion of the assumed critical surface, and residual values of the shear strength parameters were mobilized on the failed portion of that surface. The values of c_{res} and ϕ_{res} were much smaller than c_a and

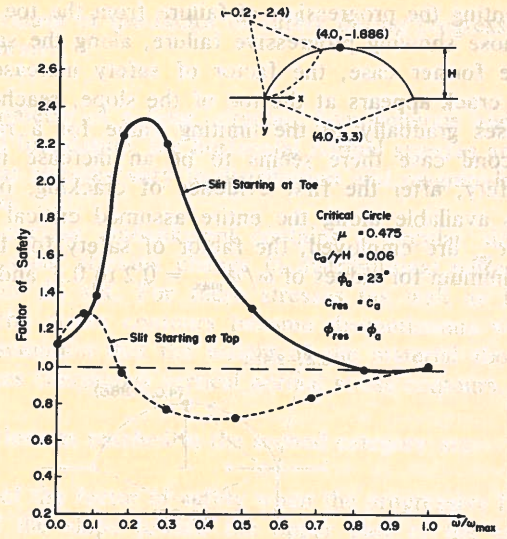

Fig. 12.—Relationship Between Factor of Safety and Progression of Slit, Case A

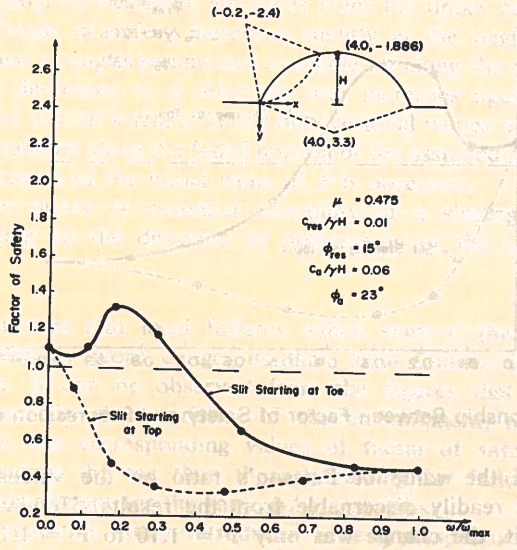

Fig. 13.—Relationship Between Factor of Safety and Progression of Slit, Case B

ϕ_a. This case is shown in Fig. 13. For Case C, peak and residual values of the shear strength parameters were available along the nonfailed and failed portions of the assumed critical surface, respectively. The value of ϕ_{res} was only slightly less than ϕ_a, but $c_{res} \to 0$. The corresponding curves appear as Fig. 14.

Curves representing the progression of failure from the toe were distinctly different from those showing progressive failure, along the same path, from the crest. In the former case, the factor of safety increases substantially shortly after the crack appears at the toe of the slope, reaches a maximum, and then decreases gradually to the limiting value for a ratio of $\omega/\omega_{max} = 1$. In the second case there seems to be an increase in the value of the factor of safety, after the first evidence of cracking, only when peak shear strength is available along the entire assumed critical surface. When values ϕ_{res} and c_{res} are employed, the factor of safety for the second case decreases to a minimum for values of $\omega/\omega_{max} = 0.2$ to 0.5, and then increases.

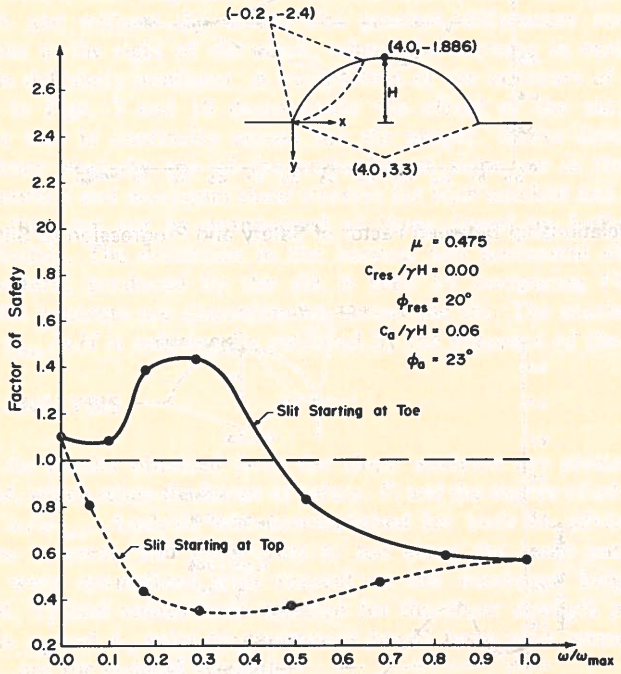

Fig. 14.—Relationship Between Factor of Safety and Progression of Slit, Case C

The effect of the value of Poisson's ratio on the values of the factor of safety is not readily discernable from the results. However, in a typical case with no slit, the change was only $F = 1.10$ to $F = 1.14$, as Poisson's ratio changed from $\mu = 0.3$ to $\mu = 0.475$.

CONCLUSIONS

The conclusions drawn from this work can be separated into two categories, viz., those concerning the magnitude and distribution of stresses, and those concerning the values of the factor of safety during progressive failure. With respect to the former:

1. For the geometry of a long, circular, homogeneous and linearly elastic embankment and foundation, the horizontal normal stresses and the horizontal and vertical shear stresses vary in distribution and magnitude with the value of Poisson's ratio.
2. When the circular embankment contains a circular slit the horizontal normal and the shear stresses change in distributional pattern as compared with the case for no slit. For these stresses (as well as for the maxima shear stresses) the stress contours become discontinuous when they cross the slit. The assumption that the weight of the material above the slit acts across it, produces continuous vertical normal stress contours.

The main conclusions reached in the second category are:

1. The values of the factor of safety when the progressive failure advanced from the toe of the slope toward the upper part of the embankment are characterized by a sharp increase for values of the ratio, ω/ω_{max}, between 0.2 and 0.3. Thereafter the value of F decreases steadily to the value for a simultaneous failure as analyzed by the method of slices.
2. When the progressive failure advances from the upper part of the slope downward the factor of safety increases slightly at the beginning for peak values of the shear strength parameters available all along the potential failure surface. It then decreases to a minimum and increases again to the value for a full assumed critical surface. When only residual values of shear strength parameters are available along the failed portion of the assumed critical surfaces, no significant increase of the initial value of F is observed.
3. The relative safety or potential instability of a sloping mass is very different depending on the direction of progression of the assumed critical surface.

This study indicates that local failures which start at the upper part of a slope are potentially more dangerous than local failures initiated at the toe of the slope. It can be observed from the figures that for the same failure path, geometric characteristics of the embankment, and parameters of shear strength, the corresponding values of factor of safety are greater for failures started at the toe than those occurring for failures starting at the top of the embankment for the same ω/ω_{max} values.

It is believed that this study introduces a new perspective in the study of the stability of sloping earth masses, and possibly in other problems involving a potential for progressive failure, namely, that the direction from which failure propagates is an important factor to consider in stability.

ACKNOWLEDGMENTS

This study was made possible by a David Ross Grant from the Purdue

University Research Foundation, whose support is gratefully acknowledged.

APPENDIX I.—REFERENCES

1. Bishop, A. W., "The Stability of Earth Dams," thesis presented to the University of London, at London, England, in 1952, in partial fulfillment of the requirements for the degree of Doctor of Philosophy.
2. Bishop, A. W., "The Use of the Slip Circle in the Stability Analysis of Slopes," *Geotechnique*. Vol. 5, No. 1, 1955, pp. 7-17.
3. Bishop, A. W., and Morgenstern, N., "Stability Coefficients for Earth Slopes," *Geotechnique*, Vol. 10, No. 4, 1960.
4. Bjerrum, L., "Progressive Failure in Slopes of Overconsolidated Plastic Clay and Clay Shales," *Journal of the Soil Mechanics and Foundations Division*, ASCE, Vol. 93, No. SM5, Proc. Paper 5456, Sept., 1967, pp. 1-49.
5. Duncan, J. M., and Dunlop, P., "Slopes in Stiff-Fissured Clays and Shales," *Journal of the Soil Mechanics and Foundations Division*, ASCE,Vol. 95, No. SM2, Proc. Paper 6449, March, 1969, pp. 467-492.
6. "Landslides and Engineering Practice," *Special Report 29*, Highway Research Board, National Academy of Sciences-National Research Council, Washington, D.C., 1958.
7. Lambe, T. W., and Whitman, R. V., *Soil Mechanics*, John Wiley & Sons, Inc., New York, N.Y., 1969.
8. LaRochelle, P., "The Short Term Stability of Slopes in London Clay," thesis presented to the University of London, at London, England, in 1960, in partial fulfillment of the requirements for the degree of Doctor of Philosophy.
9. Muskhelishvili, N. I., *Some Basic Problems of the Mathematical Theory of Elasticity*, Translated from the Russian by J. R. M. Radok. P. Noordhoff Ltd., Groningen, The Netherlands, 1963.
10. Perloff, W. H., Baladi, G. Y., and Harr, M. E., "Stress Distribution Within and Under Long Elastic Embankments," *Joint Highway Research Project Report No. 14*, Purdue University, Indiana, June, 1967.
11. Romani, F., "Dependence of Stability of Slopes on Initiation and Progression of Failure," thesis presented to Purdue University, at Lafayette, Indiana, in 1970, in partial fulfillment of the requirements for the degree of Doctor of Philosophy.
12. Terzaghi, K., and Peck, R. B., *Soil Mechanics in Engineering Practice*, 2nd ed. John Wiley & Sons, Inc., New York, N.Y., 1967.

APPENDIX II.—NOTATION

The following symbols are used in this paper:

c, ϕ = shear strength parameters;
H = maximum height of circular embankment;
t = complex variable $\xi + i\eta$ (t-plane);
u = complex variable $u_x + iu_y$ (u-plane);
w = complex variable $w_x + iw_y$ (w-plane);
x, y = Cartesian coordinates;
x_c, y_c = coordinates of center of circular arc defining contour of circular slit in z-plane;
x_o, y_o = coordinates of center of circular arc defining boundary of circular embankment in z-plane;
x_{tip}, y_{tip} = coordinates of tip of slit in z-plane;

z = complex variable $x + iy$ (z-plane);
γ = unit weight;
μ = Poisson's ratio;
ξ, η = orthogonal curvilinear coordinates in z-plane; rectangular coordinates in t-plane;
σ_x, σ_y = total normal stress components parallel to x and y axes;
τ_{xy} = shearing stress components in z-plane;
$\phi(t), \psi(t)$ = complex potentials; functions of complex variable $t = \xi + i\eta$;
$\phi(z), \psi(z)$ = complex potentials; functions of complex variable $z = x + iy$; and
ω = angular measure of slit development, ω_{max} is full development.